Simulations of Mach 0.8 Transonic Truss-Braced Wing Aircraft Aerodynamics at High Angles of Attack

Juntao Xiong*
KBR Wyle, Inc., Moffett Field, CA 94035
Nhan Nguyen†
NASA Ames Research Center, Moffett Field, CA 94035

This paper presents numerical simulations of the Mach 0.8 Transonic Truss-Braced Wing (TTBW) aircraft at high angle of attack using CFD solver FUN3D. Three different approaches - steady Reynolds Averaged Navier-Stokes (RANS), Unsteady Reynolds Averaged Navier-Stokes (URANS), and Delayed Detached Eddy Simulation (DDES) are used to simulation the TTBW aircraft at Mach number 0.8 and altitude $40,000$ ft. The pitch break phenomenon is observed at this flight condition. The simulation results show that the pitch break angle of attack occurs at $2.75°$ by DDES, $2.81°$ by URANS, and $2.89°$ by RANS. The DDES unsteady pressure begins to grow at angle of attack of $3.5°$, which might indicate the buffet onset, and rises one order of magnitude larger at angle of attack of $4.0°$. However the URANS unsteady pressure begins to grow at angle of attack of $4.0°$. Both unsteady simulation results show the pitch break occurs before buffet onset.

I. Introduction

The Subsonic Ultra Green Aircraft Research (SUGAR) Transonic Truss-Braced Wing (TTBW) aircraft concept is a Boeing-developed N+3 aircraft configuration funded by NASA Aeronautics Research Mission Directorate (ARMD) Advanced Air Transport Technologies (AATT) project.[1,2,3] The Mach 0.8 Transonic Truss-Braced Wing (TTBW) aircraft is shown in Figure 1. The TTBW aircraft design idea is to use truss structures to alleviate the wing root bending moment, so that a significant increase in the wing aspect ratio is feasible. The design of a truss-braced wing is a Multidisciplinary Design Analysis and Optimization (MDAO) process that strives to achieve a delicate balance between aerodynamic and structural efficiencies. A typical MDAO process uses a variety of different tools of varying fidelity for many different purposes such as aerodynamic prediction, aero-structural analysis, flutter analysis. Nowadays the Computational Fluid Dynamics (CFD) is an efficient method for the aerodynamic prediction and analysis.

Stability is one of the important requirements in aircraft design. Stable aircraft response without active feedback control is a desired attribute in transport aircraft design. Aircraft stability depends on many factors but the horizontal and vertical tail sizes play significant roles in providing stable aircraft design. For longitudinal motion, aircraft longitudinal static stability requires the pitching moment curve slope C_{m_α} to be negative. The pitching moment is contributed by both the wing and the horizontal tail. Tail sizing provides both static and dynamic pitch stability. The location of the aircraft center of gravity (CG) also plays an important role. Typically, the CG of an aircraft locates slightly ahead of the aerodynamic center based on the mean aerodynamic chord (MAC). This results in a nose-down pitching moment contribution by the wing lift. As the angle of attack increases, the sectional lift along the wing span reduces as the flow becomes more nonlinear due to a stall onset. Usually, stall onset tends to occurs near the wing tip for swept wing aircraft. The stall characteristic progressively moves inboard with further increase in the angle of attack. The lift reduction at the wing outboard sections results in a net decrease in the nose-down pitching moment contribution by the wing which offsets the nose-down pitching moment contribution by the horizontal tail. Pitch break occurs where the pitching moment switches the direction at a specific angle of attack which corresponds to $C_{m_\alpha} = 0$. As the angle of attack increases, eventually a nose-up pitching moment occurs, thereby potentially causing an aircraft to enter deep stall if flight control surfaces do not provide sufficient feedback action to cancel out the nose-up pitching moment. The nose-up pitching moment due to the increasing angle of attack creates a static pitch instability. So it is necessary to analyze the aerodynamic behavior at high angle of attack for an aircraft design.

*Aerospace Engineer, Intelligent System Division, juntao.xiong@nasa.gov, AIAA Member
†Senior Research Scientist and Technical Group Lead, Intelligent Systems Division, nhan.t.nguyen@nasa.gov, Associate Fellow AIAA

Figure 1 Boeing SUGAR Mach 0.8 Transonic Truss-Braced Wing (TTBW) Aircraft Concept

In this paper a series of steady and unsteady simulations of the Mach 0.8 TTBW aircraft are conducted using the CFD solver FUN3D to study the aircraft aerodynamic behaviors at high angle of attack. First, the CFD solver FUN3D simulation results of the Mach 0.8 TTBW aircraft are validated with NASA Ames 11-Ft transonic wind tunnel experimental measurements. Then, three different approaches - steady Reynolds Averaged Navier-Stokes (RANS), Unsteady Reynolds Averaged Navier-Stokes (URANS), and Delayed Detached Eddy Simulation (DDES) are used to simulate the aircraft at Mach number 0.8 and altitude $40,000$ ft. The predicted aerodynamics by the three approaches are compared and analyzed. The unsteady pressure Root Mean Square (RMS) is used to determine the buffet onset.

II. Computational Approach

A. Numerical Code

The computational fluid dynamics code used in this study is FUN3D,[5,6] which solves the unsteady three-dimensional Navier-Stokes equations on mixed-element grids using a vertices-centered finite-volume method. Information exchange for flow computation on different partitions using multiple CPUs is implemented through the MPI (Message Passing Interface) protocol. It employs an implicit upwind algorithm in which the inviscid fluxes are obtained with a flux-difference-splitting scheme. At interfaces delimiting neighboring control volumes, the inviscid fluxes are computed using an approximate Riemann solver based on the values on either side of the interface. The Roe flux difference splitting[7] is used in the current study. For second-order accuracy, interface values are obtained by extrapolation of the control volume centroidal values, based on gradients computed at the mesh vertices, using an unweighted least squares technique. The Venkatakrishnan[8] limiter is used in the current study to limit the reconstructed values when necessary. In this study the tetrahedral mesh with prism layers are used. In FUN3D, for tetrahedral meshes, the full viscous fluxes are discretized using a finite-volume formulation in which the required velocity gradients on the dual faces are computed using the Green-Gauss theorem. The solution at each time-step is updated with a backwards Euler time-differencing scheme. At each time step, the system of equations is approximately solved with either a multi-color point-implicit procedure or an implicit-line relaxation scheme. Local time-step scaling is employed to accelerate convergence to steady-state. To model turbulent flows, the one-equation model of Spalart-Allmaras[9] (S-A) is used in this study. The DDES[10] model is used for unsteady simulation.

B. Computational Model and Grid

In this paper, the Mach 0.8 TTBW 1g cruise shape geometry aircraft is used in the study. Figure 2 illustrates the Mach 0.8 TTBW geometry. Figure 3 shows the surface mesh of the Mach 0.8 TTBW geometry. The volume meshes are comprised of tetrahedral elements and a prism layer near the wall. The mesh size is about 198 million nodes for the Mach 0.8. The prism layer is used to resolve the turbulent boundary layer. The $y+$ of the first cell from the wall is less than 1.

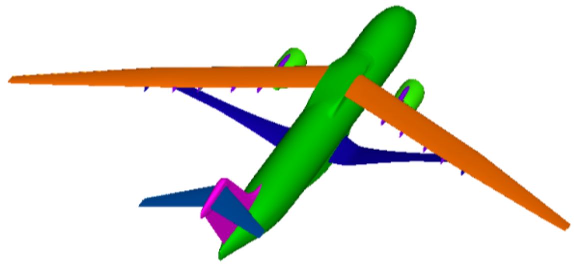

Figure 2 Mach 0.8 TTBW Aircraft Geometriy.

Figure 3 Mach 0.8 TTBW Aircraft CFD Mesh.

III. Results

Firstly, the CFD method is validated with the experimental data for the Mach 0.8 TTBW 1g geometry tested configuration, config-138 which does not include the jury strut. The wind tunnel test of the Mach 0.8 TTBW 1g model was performed in NASA Ames11-Ft Transonic Wind Tunnel. The test data from Run 679 at Mach 0.8 and Reynolds number of 1.7 million based on the mean aerodynamic chord (MAC) with full wind tunnel model corrections are used for the config-138 validation. After the validation, the steady and unsteady simulations are performed at Mach number 0.8 and altitude $40,000$ ft to study the aerodynamic behaviors at high angle of attacks of the aircraft.

A. CFD Solver Validation

The presentation of the results begins with a comparison between the aerodynamic forces and moment coefficients obtained both experimentally from a wind tunnel test in the NASA Ames 11-By-11-Foot Transonic Wind Tunnel, and computationally via FUN3D for the Mach 0.8 TTBW geometry config-138 for Mach 0.8 and a Reynolds number of 1.7 million.

To improve the comparison between the computation results and wind tunnel data, it is necessary to apply an aeroelastic twist correction at wind tunnel Reynolds number. Ideally, this should be done using NASTRAN FEM of wind tunnel model which is not available, but full-scale NASTRAN FEM is available. A correction procedure[11] was developed to estimate the aeroelastic twist correction of the wind tunnel model.

Using the developed corrections the 1G OML solution at wind tunnel Reynolds number with incremental aero coefficients at flight Reynolds is corrected to obtain estimates of the jig twist OML aero coefficients at wind tunnel Reynolds number. Figure 4 shows the lift, drag, and pitching moment coefficients computed by FUN3D as well as Run 679[13] wind tunnel data. With the developed aeroelastic model deformation correction the validation is improved. The discrepancy is reduced when the model deformation is accounted. The drag polar computed by FUN3D shows good agreement with the wind tunnel data. The discrepancy in the drag coefficient progressively becomes larger at larger lift coefficients. Figure 5 shows the surface pressure coefficient distribution at angle of attack $2°$ for Mach number 0.8 of config-138. The close agreements with wind tunnel data provide confidence in the FUN3D prediction for Mach 0.8

TTBW aircraft design.

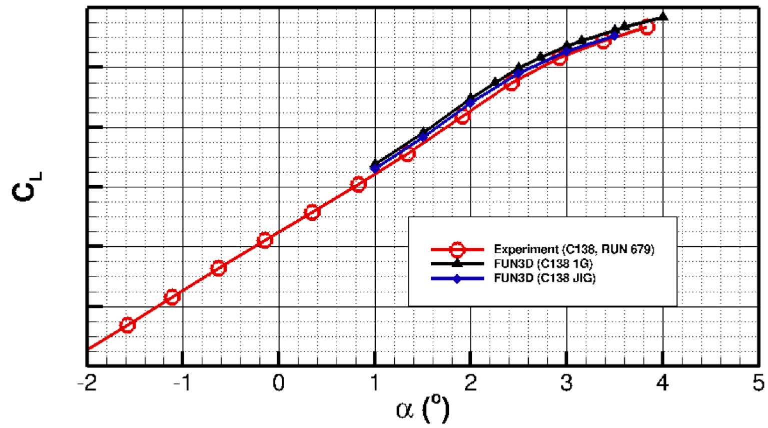

(a) Lift Curve

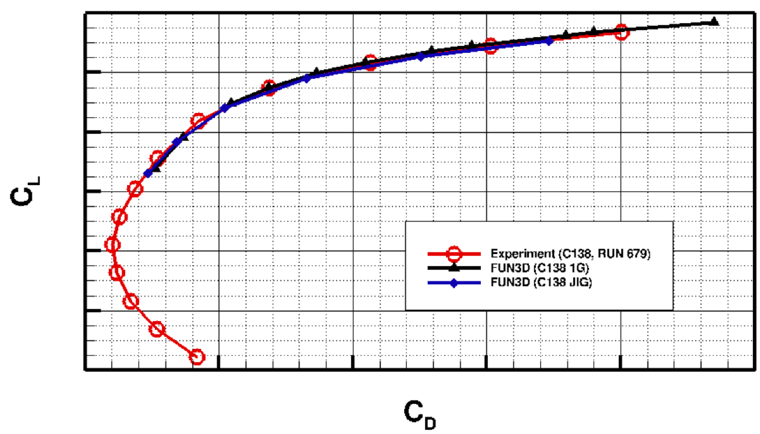

(b) Drag Polar

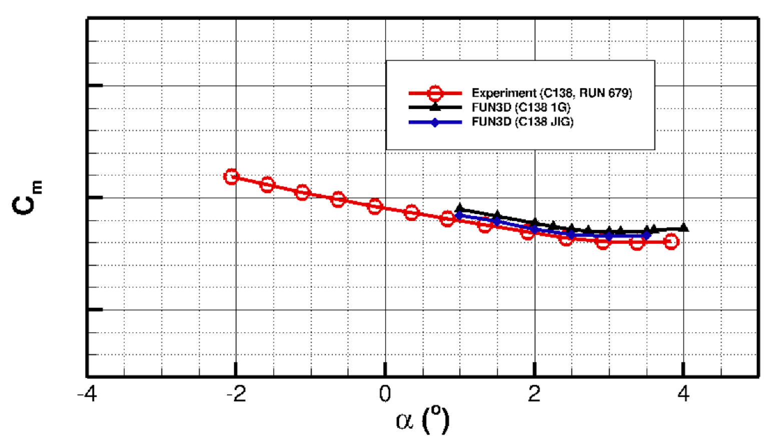

(c) Pitch Moment Curve

Figure 4 Comparison of Lift, Drag, and Pitching Moment Predictions for the TTBW Geometry Config-138 at Mach 0.8 and $Re = 1.7 \times 10^6$.

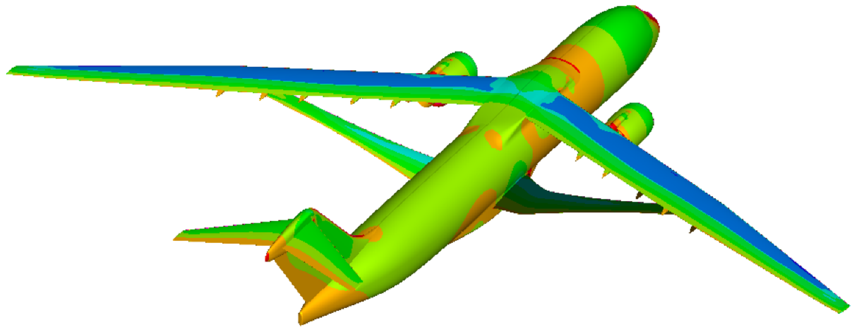

Figure 5 Pressure Coefficient Contour on the TTBW 1G Geometry Config-138 Surface at Mach 0.8, $\alpha = 2°$ and $Re = 1.70 \times 10^6$.

B. Steady-state Simulations

The trim solutions are obtained by iterating on the angle of attack and horizontal tail incidence angle at Mach 0.8, altitude 40,000 ft, and design C_L 0.695. The trim horizontal incidence angle is about $-0.75°$. Figure 6 shows the pressure contours for the Mach 0.8 TTBW at the trim condition.

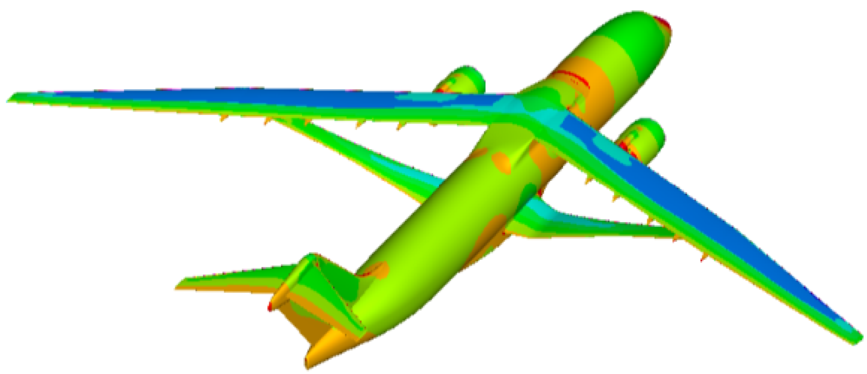

Figure 6 Pressure Coefficient Contour of the Mach 0.8 TTBW aircraft at Trim Condition.

After the trim configuration is obtained a series steady-state simulations are performed at Mach 0.8, altitude 40,000 ft, and different angle of attacks. Figure 7 shows the lift, drag, and pitching moment coefficients of the Mach 0.8 TTBW trim configuration with horizontal incidence angle $-0.75°$. The lift and drag curves show the nonlinear aerodynamic phenomenon appears and the drag rises dramatically when the angle of attack is higher than 2.5°. The pitching moment curve also shows the pitching moment starts to increase when the angle of attack is higher than 2.5°. Figure 8 shows the pitching moment coefficient derivative respect to the angle of attack. The results show that the pitching moment curve slope $C_{m_\alpha} = 0$ at angle of attack about 2.89° which indicates the pitch break. The aircraft might encounter instability issue at high angle of attacks if pitch break appears. The aircraft, wing, and tail pitching moments and pitching moments derivatives show that the pitch break seems to be largely influenced by the wing rather than the tail.

To further confirm the pitch break the aircraft is re-trimmed at angle of attack 2.89°. The re-trimmed horizontal incidence angle is about $-1.03°$ to make the full aircraft pitching moment 0 at angle of attack 2.89°. A series steady-state simulations are performed for the re-trimmed configuration at Mach 0.8 and altitude 40,000 ft. Figure 9 shows the lift, drag, and pitching moment coefficients of the Mach 0.8 TTBW re-trimmed configuration with horizontal incidence angle $-1.03°$. Figure 10 shows the pitching moment coefficient derivative respect to the angle of attack. The pitch break is also observed for the Mach 0.8 TTBW re-trimmed configuration. Figure 11 shows the relations between the pitching moment coefficient and lift coefficient for the two trim configurations. The results show that pitch break occurs at a similar lift coefficient for the two trim configurations.

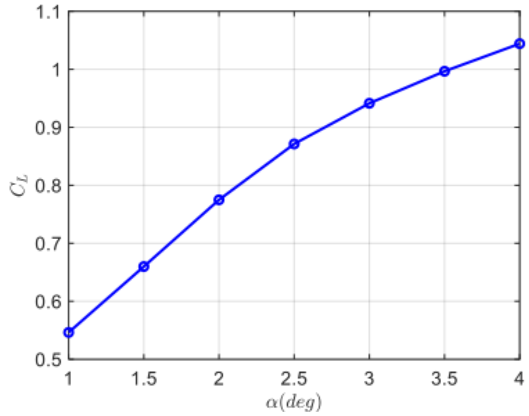

(a) Lift Curve

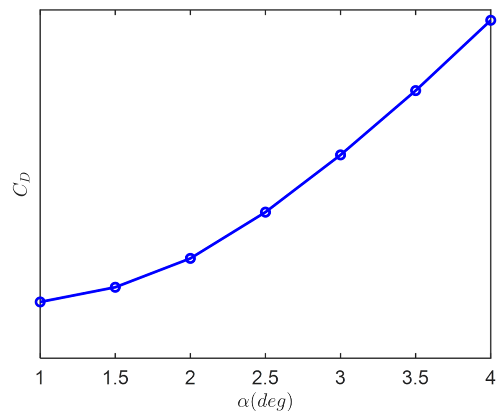

(b) Drag Curve

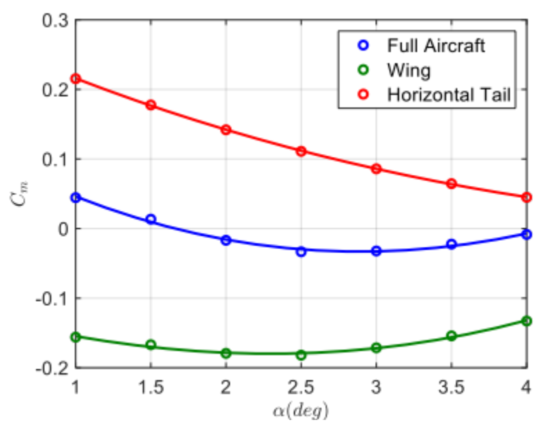

(c) Pitch Moment Curve

Figure 7 Lift, Drag, and Pitching Moment for the TTBW Geometry at Mach 0.8, h = 40,000ft, and $\delta_e = -0.75°$.

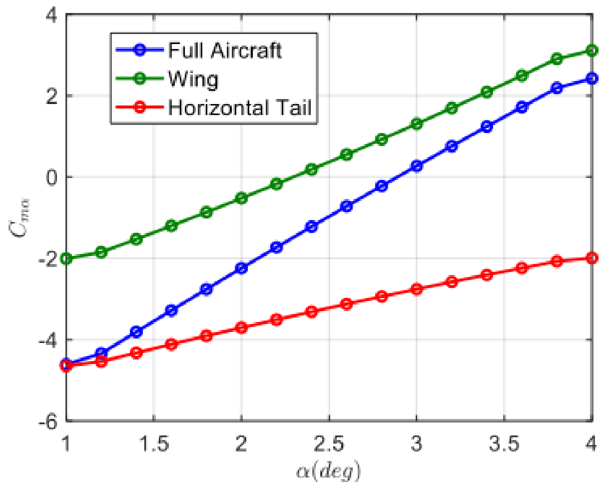

Figure 8 Pitching Moment Derivatives for the TTBW Geometry at Mach 0.8, h = 40,000ft, and $\delta_e = -0.75°$.

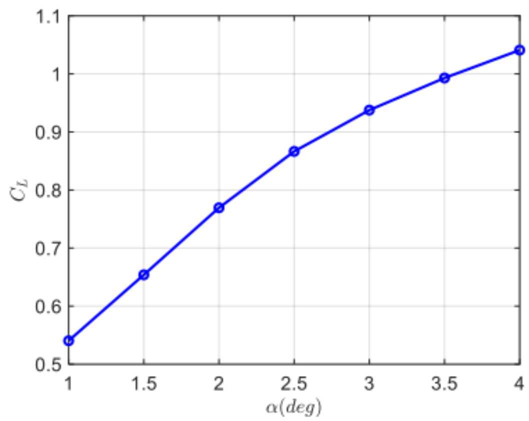

(a) Lift Curve

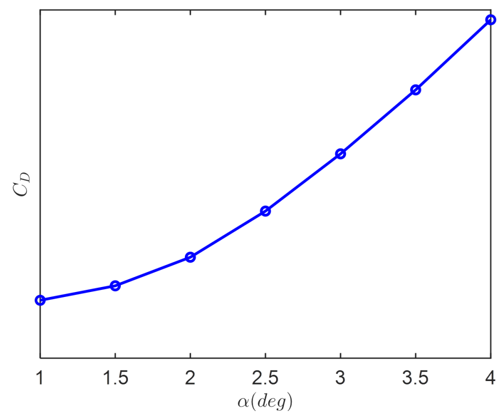

(b) Drag Curve

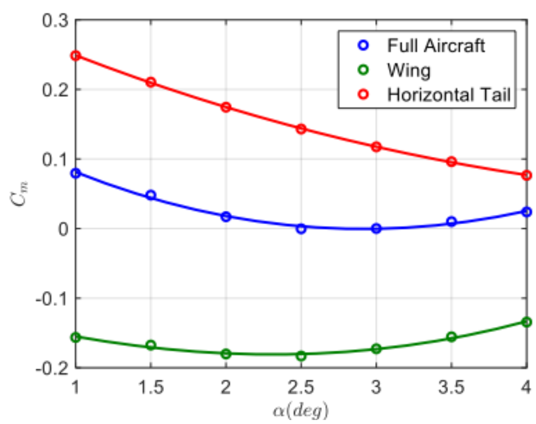

(c) Pitch Moment Curve

Figure 9 Lift, Drag, and Pitching Moment for the TTBW Geometry at Mach 0.8, h = 40,000ft, and $\delta_e = -1.03°$.

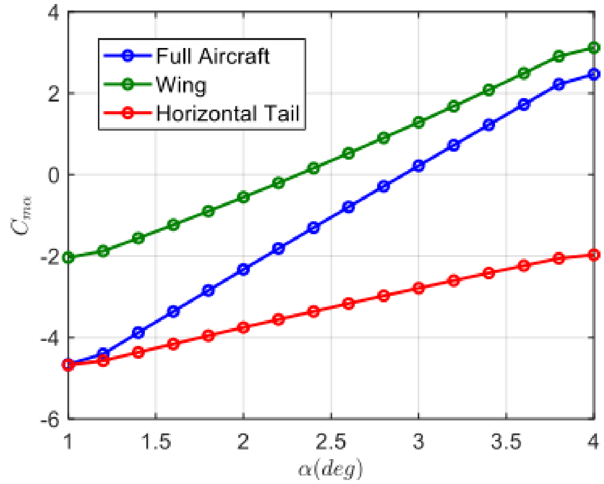

Figure 10 Pitching Moment Derivatives for the TTBW Geometry at Mach 0.8, h = 40,000ft, and $\delta_e = -1.03°$.

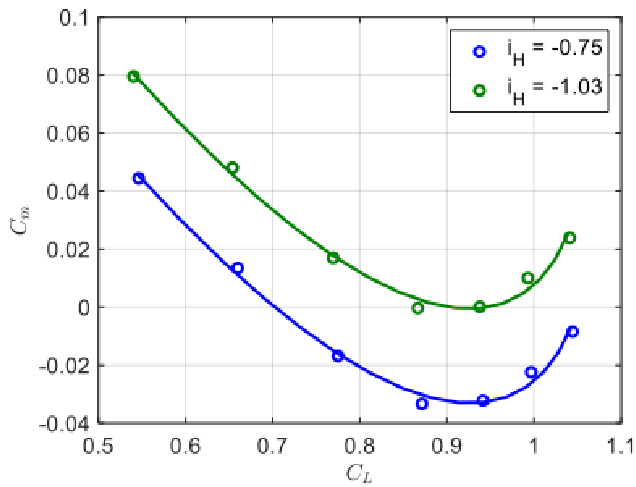

Figure 11 Pitching Moment vs lift coefficient for the TTBW Geometry at Mach 0.8, h = 40,000ft.

C. Unsteady Simulations

To further investigation the flow behavior of the Mach 0.8 TTBW aircraft at high angle of attack two different unsteady simulations URANS and DDES are performed at the trim condition with the horizontal incidence angle $-0.75°$. In the unsteady simulation the time step is about $0.00078s$ for URANS and DDES.

Figure 12 - 13 show lift coefficient history and FFT analysis for the Mach 0.8 TTBW aircraft at Mach 0.8 and angle of attack 4° using URANS and DDES. The DDES predicts smaller time-averaged lift coefficient with larger fluctuations than URANS predictions. The FFT of the URANS lift coefficient shows the dominant Strouhal number is about 0.252. The FFT of the DDES lift coefficient shows two dominant Strouhal numbers are about 0.053 and 0.172.

Figure 14 shows the instantaneous density contours for the Mach 0.8 TTBW aircraft at Mach 0.8 and angle of attack 4° using URANS and DDES. Figure 15 shows the unsteady pressure root mean square (RMS) contours for the Mach 0.8 TTBW aircraft at Mach 0.8 and angle of attack 4°. Figure 16 - 17 show the unsteady pressure RMS profiles at four spanwise locations for the Mach 0.8 TTBW aircraft at Mach 0.8 and angle of attack 4° using URANS and DDES. The URANS only capture the pressure oscillation near the wing tip region. The shock wave moves between the 35% - 60% of the local chord. There are two large pressure oscillation regions near the wing-strut juncture and wing tip computed by DDES. Near the wing-strut juncture the shock wave moves between the 35% - 60% of the local chord. Near the wing tip the shock wave moves between the 28% - 63% of the local chord. The DDES approach captures more unsteadiness than URANS.

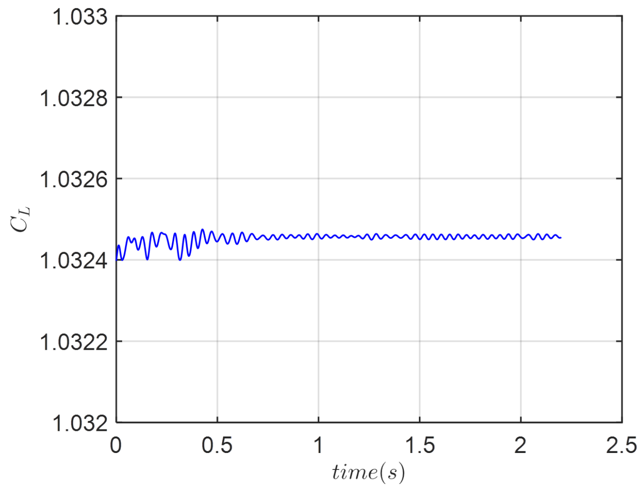

(a) URANS

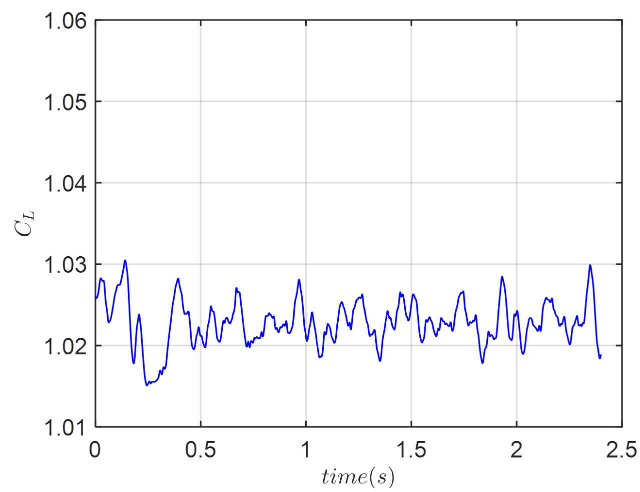

(b) DDES

Figure 12 lift coefficient history for the TTBW aircraft at Mach 0.8, h = 40,000ft and angle of attack $4°$.

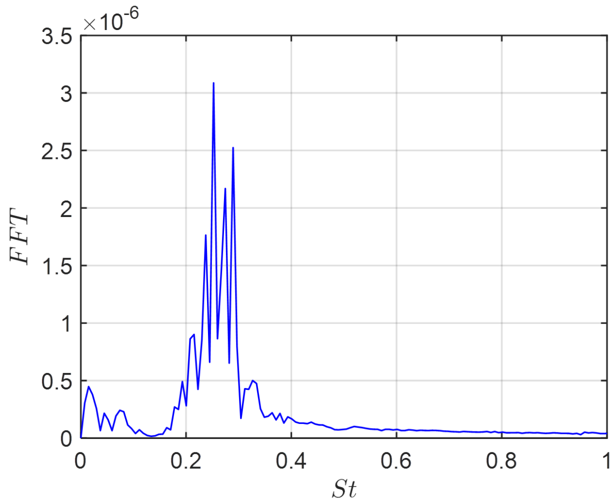

(a) URANS

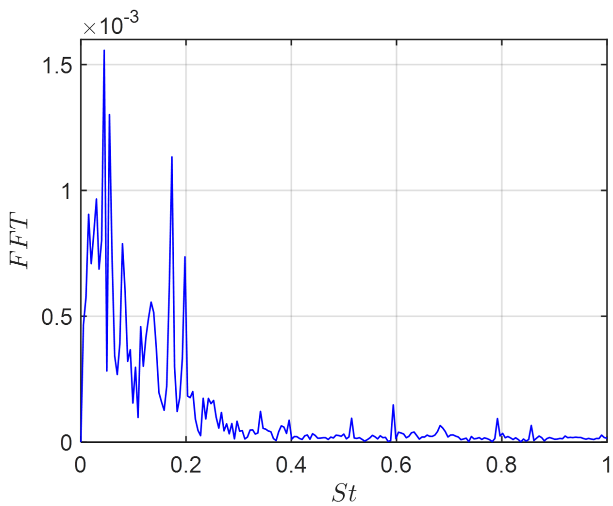

(b) DDES

Figure 13 FFT of the lift coefficients for the TTBW aircraft at Mach 0.8, h = 40,000ft and angle of attack $4°$.

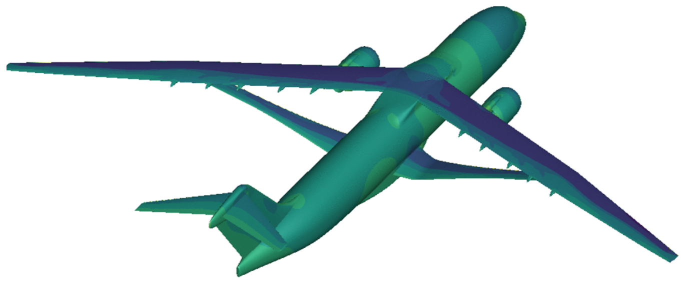

(a) URANS

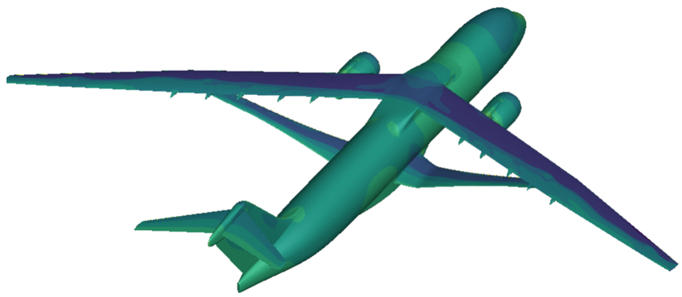

(b) DDES

Figure 14 Density Contour of the Mach 0.8 TTBW aircraft at Mach 0.8, h = 40,000ft and angle of attack 4°**.**

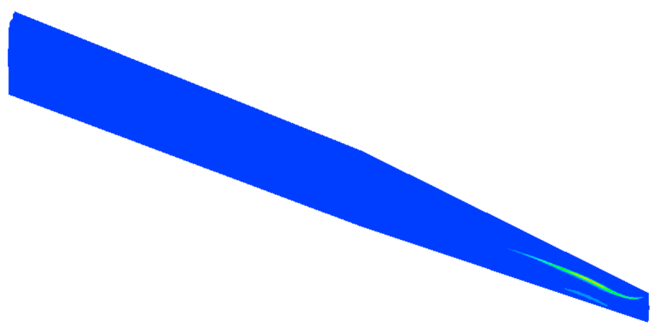

(a) URANS

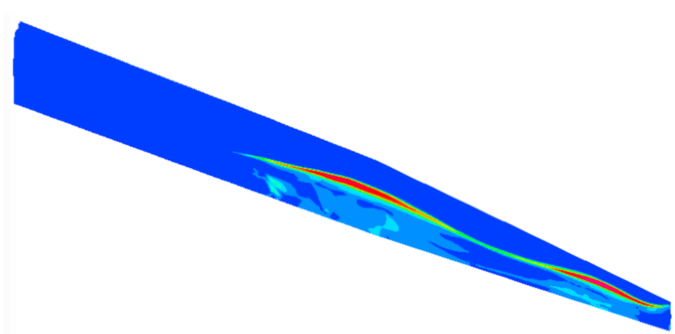

(b) DDES

Figure 15 Unsteady Pressure RMS of the Mach 0.8 TTBW aircraft at Mach 0.8, h = 40,000ft and angle of attack 4°**.**

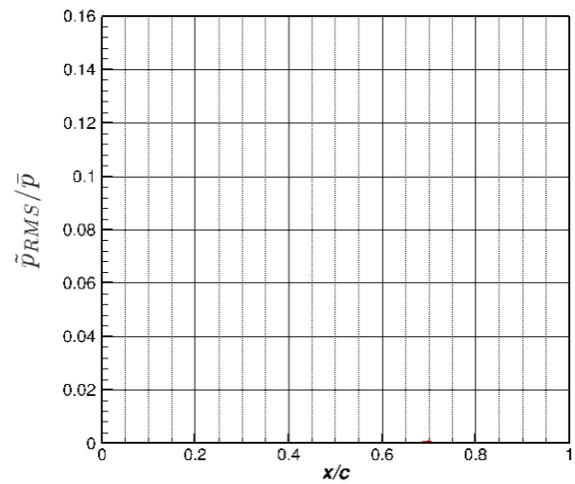

(a) η = 0.24

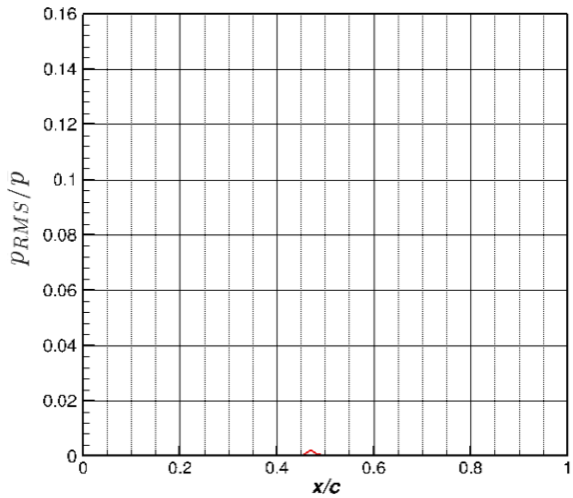

(b) η = 0.55

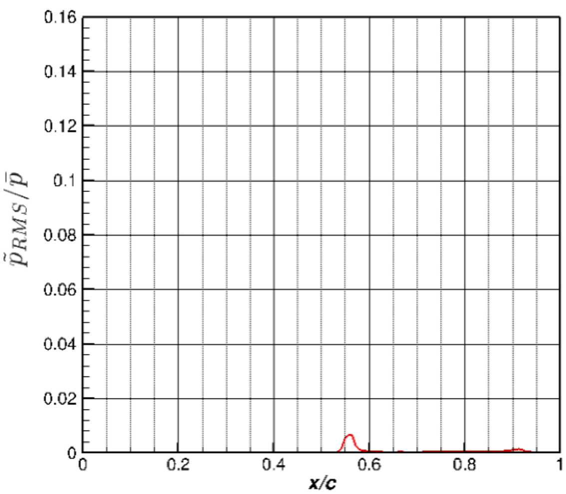

(c) η = 0.73

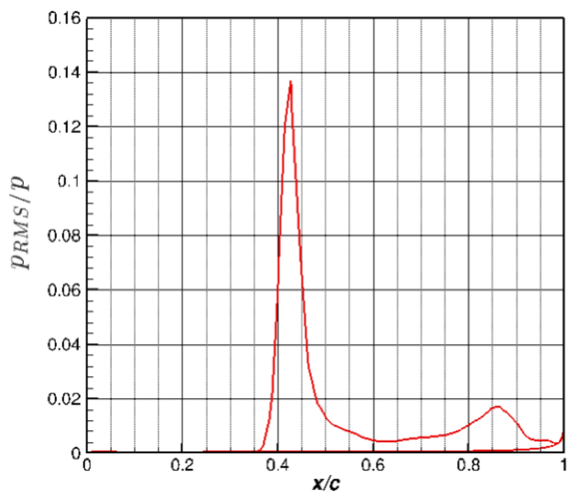

(d) η = 0.88

Figure 16 Unsteady Pressure RMS Profile of the Mach 0.8 TTBW aircraft at Mach 0.8, h = 40,000ft and angle of attack 4° using RUANS.

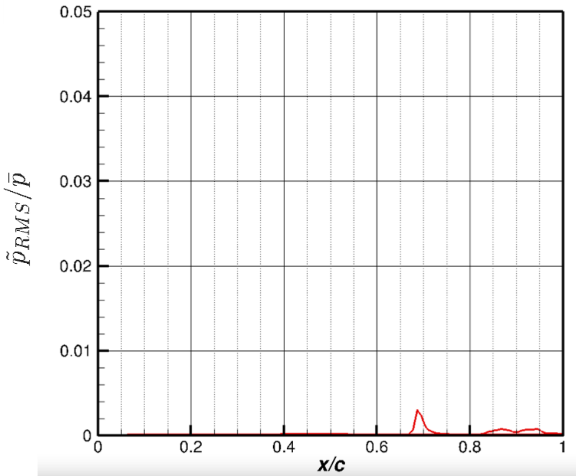

(a) η = 0.24

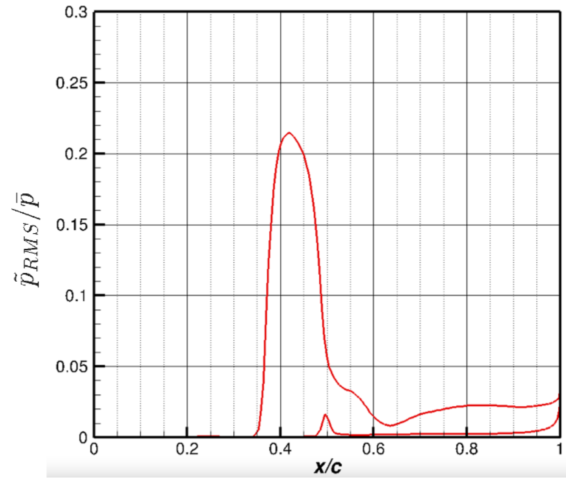

(b) η = 0.55

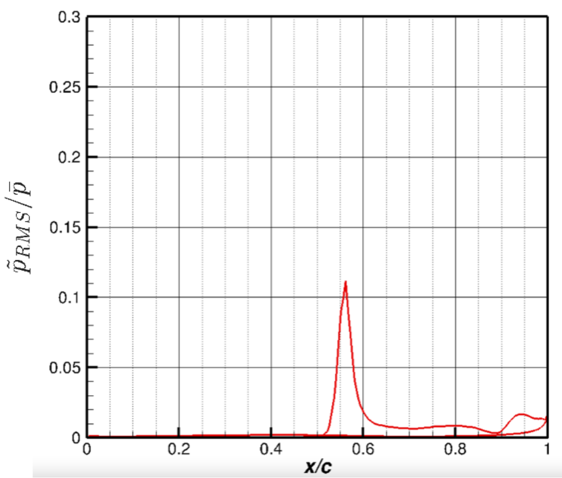

(c) η = 0.73

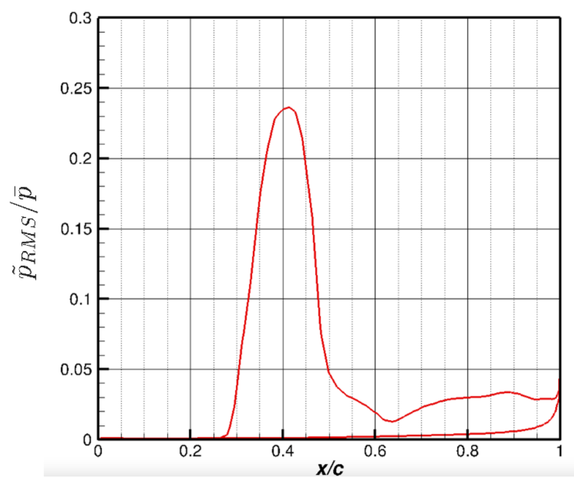

(d) η = 0.88

Figure 17 Unsteady Pressure RMS Profile of the Mach 0.8 TTBW aircraft at Mach 0.8, h = 40,000ft and angle of attack $4°$ using DDES.

Figure 18 shows the unsteady pressure peak RMS contours for the Mach 0.8 TTBW aircraft at Mach 0.8. The DDES unsteady pressure begins to grow at angle of attack of 3.5°, which might indicates the buffet onset, and rise one order of magnitude larger at angle of attack of 4.0°. The URANS unsteady pressure begins to grow at angle of attack of 4.0°.

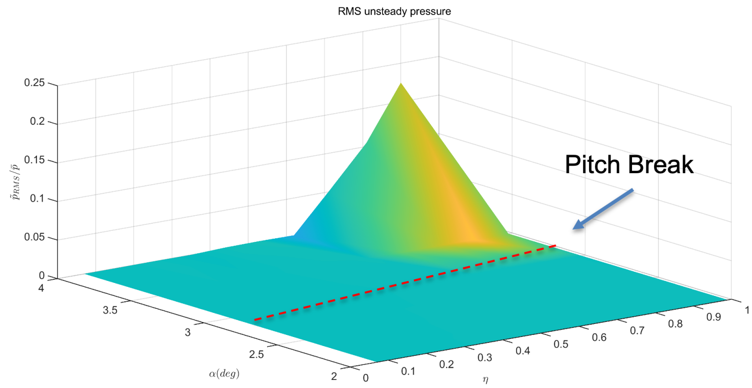

(a) URANS

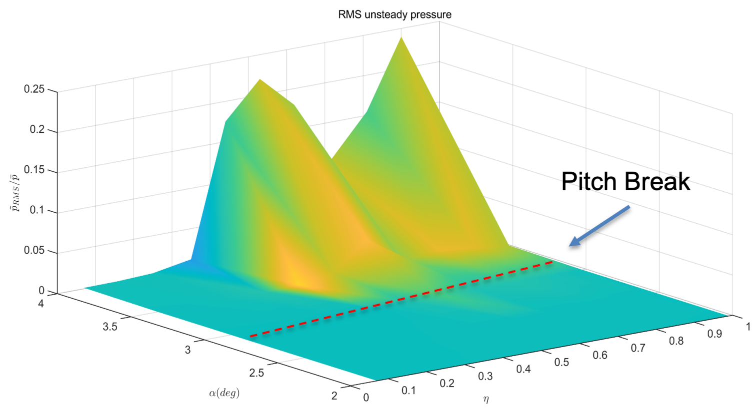

(b) DDES

Figure 18 Unsteady Pressure Peak RMS of the Mach 0.8 TTBW aircraft at Mach 0.8, h = 40,000ft.

Figure 19 shows comparisons of the lift and pitching moment coefficients of the Mach 0.8 TTBW trim configuration with horizontal incidence angle $-0.75°$ using the steady, URANS, and DDES approaches. All the three approaches show the pitch break, which confirms the pitch break behavior of the Mach 08 TTBW aircraft at high angle of attack. The results show that the pitch break angle of attack predicted at 2.75° by DDES, 2.81° by URANS, and 2.89° by RANS. The pitch break occurs before buffet onset.

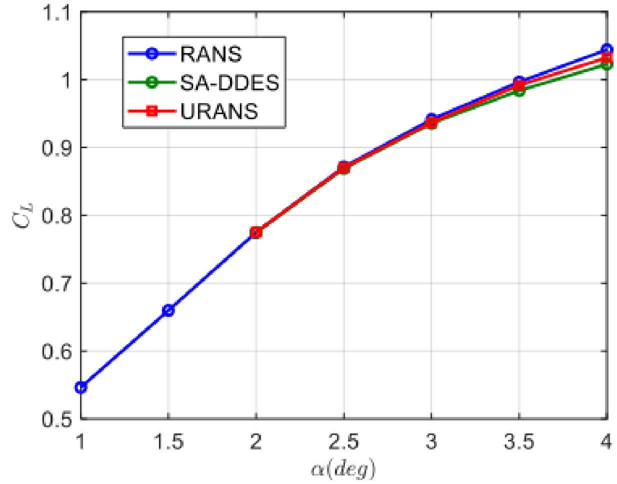

(a) Lift Curve

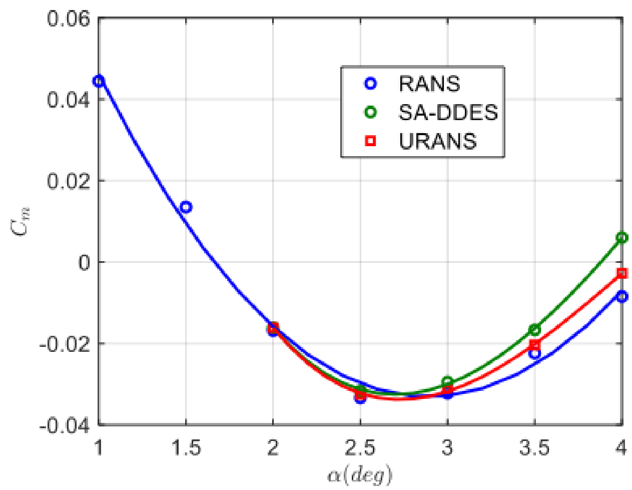

(b) Pitch Moment Curve

Figure 19 Lift and Pitching Moment for the TTBW Geometry at Mach 0.8, h = 40,000ft, and $\delta_e = -0.75°$.

Conclusions

In this paper the steady and unsteady simulations of the Mach 0.8 TTBW aircraft using the high-fidelity CFD solver FUN3D were conducted to investigate the aircraft aerodynamics at high angle of attack. The CFD solver is validated with the wind tunnel experimental data. The simulations results with the proposed aeroelastic twist correction agree well with the experimental data. The pitch break is observed from the high angle of attack simulations. The simulation results show that the pitch break angle of attack occurs at 2.75° by DDES, 2.81° by URANS, and 2.89° by RANS. The DDES unsteady pressure begins to grow at angle of attack of 3.5°, which might indicate the buffet onset, and rise one order of magnitude larger at angle of attack of 4.0°. The URANS unsteady pressure begins to grow at angle of attack of 4.0°. The pitch break occurs before buffet onset and is likely due to separated flow over wing.

Acknowledgment

The authors wish to acknowledge NASA Advanced Air Transport Technology project for the funding support of this work. The authors also acknowledge Boeing Research and Technology and in particular Christopher Droney, Neal

Harrison, Michael Beyar, Eric Dickey, and Anthony Sclafani, along with the NASA technical POC, Gregory Gatlin, for their research conducted under the NASA BAART contracts NNL10AA05B and NNL16AA04B. The research published in this paper is made possible by the technical data and wind tunnel test data furnished under these BAART contracts.

References

[1] Bhatia, M., et. al.. "Structural and Aeroelastic Characteristics of Truss-Braced Wing: A Parametric Study," Journal of Aircraft, Vol 49, No. 1, 2012.

[2] Gundlach, J. F., Tetrault, P. A., Gern, F. H., Nagshineh-Pour, A. H., Ko, A., Schetz, J. A., et. al., "Conceptual Design Studies of a Strut-Braced Wing Transonic Transport," Journal of Aircraft, Vol. 37, No. 6, 2000.

[3] Gur, O., Bhatia, M., Schetz, J.A., Mason, W. H., Kapania, R. K., and Mavris, D. N., "Design Optimization of a Truss-Braced Wing Transonic Transport Aircraft," Journal of Aircraft, Vol. 47, No. 6, 2010.

[4] Nguyen, N. and Xiong, J., "CFD-Based Frequency Domain Method for Dynamic Stability Derivative Estimation with Application to Transonic Truss-Braced Wing," AIAA Aviation Conference, AIAA-2022, June 2022.

[5] Biedron, R. T., et al., "FUN3D Manual 13.2,", NASA TM-2017-219661, Aug. 2017

[6] Lee-Rausch, E. M., Hammond, D. P., Nielsen, E. J., Pirzadeh, S. Z., and Rumsey, C. L., "Application of the FUN3D Unstructured-Grid Navier-Stokes Solver to the 4th AIAA Drag Prediction Workshop cases," AIAA Aviation Conference, AIAA-2010-4511, January 2019.

[7] Roe, P. L., "Approximate Riemann Solvers, Parameter Vectors and Difference Schemes,", Journal of Computational Physics, Vol. 46, No. 2, 1980, pp. 357-378

[8] Venkatakrishnan, V., "Convergence to Steady State Solutions of the Euler Equations on Unstructured Grids with Limiters,", Journal of Computational Physics, Vol. 118, No. 1, 1995, pp. 120-130

[9] Spalart, P. R. and Allmaras, S. R., "A One-Equation Turbulence Model for Aerodynamic Flows," AIAA Science and Technology Forum and Exposition, AIAA-1992-0439, January 1992.

[10] Spalart, P. R., Deck, S.. Shur, M. L., Squires, K. D., Strelets, M. K. and Travin, A., "A New Version of Detached-eddy Simulation, Resistant to Ambiguous Grid Densities," Theoretical and Computational Fluid Dynamics, Vol. 20, No. 3, 2006, pp. 181-195

[11] Xiong, J., Nguyen, N., and Bartels, R. E., "Jig Twist Optimization of Mach 0.8 Transonic Truss-Braced Wing Aircraft," AIAA Science and Technology Forum and Exposition, AIAA-2023-1573, Jan. 2023.

[12] Xiong, J., Nguyen, N., and Bartels, R. E., "Aeroelastic Analysis of Mach 0.8 Transonic Truss-Braced Wing Aircraft," AIAA Science and Technology Forum and Exposition, AIAA-2022-0300, Jan. 2022.

[13] Harrison, N. A., Sclafani, A. J., Beyar, M. D., Dickey, E. D., and Intravartolo, N. M., "Subsonic Ultra Green Aircraft Research: Phase *IV* Final Report: Vol.2 Transonic Truss-Braced Wing High-Speed Test Report, " NASA/CR-2020-000000, 2020.

[14] Xiong, J., Nguyen, N., and Bartels, R. E., "Aerodynamic Optimization of Mach 0.8 Transonic Truss-BracedWing Aircraft using Variable Camber Continuous Trailing Edge Flap," AIAA Science and Technology Forum and Exposition, AIAA-2022-0016, Jan. 2022.